

# Quantum Risk Analysis: Beyond (Conditional) Value-at-Risk

Christian Laudagé<sup>\*a</sup> and Ivica Turkalj<sup>†b</sup>

<sup>a</sup>Department of Mathematics, RPTU Kaiserslautern-Landau,  
Gottlieb-Daimler-Straße 47, 67663 Kaiserslautern

<sup>b</sup>Department of Financial Mathematics, Fraunhofer Institute for  
Industrial Mathematics ITWM, Fraunhofer-Platz 1, 67663  
Kaiserslautern, Germany

March 15, 2024

## Abstract

Risk measures are important key figures to measure the adequacy of the reserves of a company. The most common risk measures in practice are Value-at-Risk (VaR) and Conditional Value-at-Risk (CVaR). Recently, quantum-based algorithms are introduced to calculate them. These procedures are based on the so-called quantum amplitude estimation algorithm which lead to a quadratic speed up compared to classical Monte-Carlo based methods.

Based on these ideas, we construct quantum-based algorithms to calculate alternatives for VaR and CVaR, namely the Expectile Value-at-Risk (EVaR) and the Range Value-at-Risk (RVaR). We construct quantum algorithms to calculate them. These algorithms are based on quantum amplitude estimation. In a case study, we compare their performance with the quantum-based algorithms for VaR and CVaR. We find that all of the algorithms perform sufficiently well on a quantum simulator. Further, the calculations of EVaR and VaR are robust against noise on a real quantum device. This is not the case for CVaR and RVaR.

KEYWORDS: Risk measures, expectiles, Range Value-at-Risk, quantum computing, quantum amplitude estimation

---

<sup>\*</sup>*E-mail:* christian.laudage@rptu.de (corresponding author).

<sup>†</sup>*E-mail:* ivica.turkalj@itwm.fraunhofer.de.

# 1. Introduction

Risk measures are important key figures used by financial institutions to assess their financial positions. The most common risk measures used in practice are the Value-at-Risk and the Conditional Value-at-Risk. In most of the cases, they are calculated by time-consuming Monte-Carlo based methods. In contrast, Woerner and Egger (2019) use the so-called quantum amplitude estimation to calculate the Value-at-Risk and the Conditional Value-at-Risk. Compared to classical Monte-Carlo methods, this approach promises a quadratic reduction of the computation time.

There are reasonable alternatives for the Value-at-Risk and Conditional Value-at-Risk and to the best of our knowledge, they have not been calculated on a quantum computer until now. We would like to fill this gap for the following two alternatives: First, the Expectile Value-at-Risk and second, the Range Value-at-Risk. The Expectile Value-at-Risk is based on the statistical concept of expectiles.

**State-of-the-art:** Expectiles are introduced originally in Newey and Powell (1987) and they enjoy new interest in the last decade, see e.g., Bellini and Di Bernardino (2017) and Bellini et al. (2014), as well as, the references therein. An expectile can be seen as a generalized mean and the term “expectile” is a combination of the words expectation and quantile. Hence, it is a compromise between Value-at-Risk and Conditional Value-at-Risk. Further, it is a special case of a shortfall risk measure as defined in, e.g., Föllmer and Schied (2016).

In contrast to the Value-at-Risk, the Conditional Value-at-Risk takes the amount of losses into account for calculating capital requirements. But the Expected Shortfall is not qualitatively robust, i.e., if there are small perturbations in the law of the underlying data, then the law of the Conditional Value-at-Risk estimator can change significantly. A qualitatively robust risk measure that takes the amount of losses into account is the Range Value-at-Risk. It is introduced in Cont et al. (2010). For further studies including the Range Value-at-Risk see Embrechts et al. (2020) and Fissler and Ziegel (2021).

We suggest procedures for the calculation of expectiles and Range Value-at-Risk by using quantum amplitude estimation. For an introduction to quantum amplitude estimation we refer to Kaye et al. (2007). The application of quantum computing to solve tasks in financial mathematics is quite new. For an overview we refer to Egger et al. (2020). Option pricing with the help of amplitude estimation is performed in Stamatopoulos et al. (2020) and Chakrabarti et al. (2021). Market risk of financial derivatives are determined via quantum computing in Stamatopoulos et al. (2022). The only algorithms for calculating risk measures are developed in Woerner and Egger (2019). These algorithms are applied to calculate credit risk in Egger et al. (2021).

**Methodology:** An expectile can be formulated as the root of a specific function including an expectation. The idea of computing expectiles by a quantum algorithm stems from the tractability of this function on a quantum computer. Hence, we calculate this function by amplitude estimation and perform a root search algorithm on a classical computer. In contrast, the Range Value-at-Risk is directly calculated as the result of an amplitude estimation.

**Contributions of this manuscript:** Our contributions are twofold. First, the ideas

to calculate Value-at-Risk and Conditional Value-at-Risk in Woerner and Egger (2019) are transferred to build up new algorithms for expectiles and Range Value-at-Risk. Second, we calculate these risk measures, as well as, Value-at-Risk and Conditional Value-at-Risk for normal, lognormal and gamma distributions and compare their performance.

We find that the algorithms converge in an adequate manner depending on the number of qubits used for loading the distribution. Further, the efficiency of noisy intermediate-scale quantum devices are evaluated by applying different variants of the amplitude estimation on a real quantum computer, namely the IBMQ Kolkata device. The expectile calculation is robust against the noise of the real quantum hardware and an iterative variant of the amplitude estimation leads to the lowest estimation errors. In contrast, the results for the Range Value-at-Risk are significantly affected by the noise of the quantum device.

**Structure of this manuscript:** In Section 2, we introduce the risk measures of interest. In Section 3, we state the algorithms for expectiles and Range Value-at-Risk. In Section 4, the implementation of the operators used in the quantum amplitude estimation is described. In Section 5, we compare the performance of the algorithms for Value-at-Risk, Conditional Value-at-Risk, expectiles and Range Value-at-Risk via a numerical case study. Some technical facts and additional figures are shifted to Appendix A and B. For the sake of completeness, the mathematical background of the analyzed risk measures and properties of expectiles that are important for applying the root search algorithm are stated in Appendix C.

## 2. Risk measures

We start by explaining the idea behind a risk measure. In practice, risk measures are used as key figures to describe the risk of a future unknown financial position. The value of a risk measure can then be interpreted as a capital reserve.

Woerner and Egger (2019) discussed the Value-at-Risk (VaR) and the Conditional Value-at-Risk (CVaR). The latter coincides with the so-called Expected Shortfall (ES) in case of a continuous random variable. We aim to discuss two more risk measures, namely the Expectile Value-at-Risk (EVaR) and the Range Value-at-Risk (RVaR).

In the following, we explain how they are calculated for a continuous random variable  $X$  and mention their main characteristics. Probabilities are denoted by  $P(\cdot)$  and expectations are denoted by  $E[\cdot]$ . For completeness, we state the mathematical definitions in Appendix C.

**VaR:** The VaR at level  $0 < \lambda < 1$  is the negative value of the  $\lambda$ -quantile of the random variable  $X$ . We denote this value by  $\text{VaR}_\lambda(X)$ . Hence, it holds that

$$P(X \leq -\text{VaR}_\lambda(X)) = P(X + \text{VaR}_\lambda(X) \leq 0) = \lambda.$$

So, by using the VaR as capital reserve, the value of the total position  $X + \text{VaR}_\lambda(X)$  is only in  $\lambda$ -percent of the cases negative, i.e., in only  $\lambda$ -percent of the cases, a loss occurs.

But, the VaR does not encourage the diversification of a portfolio in general, i.e., diversification does not lead to a decrease of the capital reserve in general. Further, the VaR does not take the amount of losses into account. To avoid these undesirable effects, the CVaR became quite popular in practice.

**CVaR:** The CVaR at level  $0 < \lambda < 1$  takes the amount of losses into account in the sense that it is the negative conditional expectation of the random variable  $X$ , conditioned on the event that the value of  $X$  is lower than  $-\text{VaR}_\lambda(X)$ . We denote this value by  $\text{CVaR}_\lambda(X)$  and it is given by

$$\text{CVaR}_\lambda(X) = E[-X \mid X \leq -\text{VaR}_\lambda(X)].$$

So, the CVaR gives us the negative average of the  $\lambda$ -percent worst scenarios of  $X$ .

**EVaR:** The EVaR is a valid alternative to the commonly used VaR and CVaR. The EVaR is the negative value of a so-called expectile. The word expectile is a combination of the words expectation and quantile. As stated by Bellini and Di Bernardino (2017), “expectiles can be seen as an asymmetric generalization of the mean” and we can interpret them as a compromise between VaR and CVaR. We use the following quote from Bellini and Di Bernardino (2017) to motivate that expectiles are good alternatives for VaR and CVaR:

“Theoretical and numerical results indicate that expectiles are perfectly reasonable alternatives to VaR and ES risk measures.”

The expectile at level  $0 < \alpha < 1$  of the random variable  $X$  is denoted by  $e_\alpha(X)$  and it is the solution of the following equation:

$$\alpha E[\max\{X - e_\alpha(X), 0\}] = (1 - \alpha)E[-\min\{X - e_\alpha(X), 0\}]. \quad (2.1)$$

A good interpretation of this value is given in the case of  $E[|X - e_\alpha(X)|] \neq 0$ . Then, we can rewrite the previous equation as

$$\alpha = \frac{E[-\min\{X - e_\alpha(X), 0\}]}{E[|X - e_\alpha(X)|]}.$$

Hence, the expectile is the value for which the expected loss of  $X - e_\alpha(X)$  only accounts for  $\alpha$ -percent of the total deviations of  $X - e_\alpha(X)$  from zero. So, we can interpret  $-e_\alpha(X)$  as a capital reserve and this is exactly the EVaR, which we denote by  $\text{EVaR}_\alpha(X) = -e_\alpha(X)$ .

**RVaR:** An important property for the application of risk measures is qualitative robustness. It describes roughly that small changes in the law of the observed data points should not lead to drastically changes in the law of the risk estimator. Changes are measured by an appropriate metric. For a precise definition of qualitative robustness

in the context of risk measures we refer to Cont et al. (2010), Koch-Medina and Munari (2022), and Krätschmer et al. (2014).

The VaR is qualitatively robust, while the CVaR is not. But the CVaR takes the magnitude of losses into account. As a compromise, one can use the RVaR, which admits desirable robustness properties in the sense of Cont et al. (2010) and takes the amount of losses partly into account.

The RVaR is defined for two levels  $0 < \alpha < \beta < 1$ . We denote it by  $\text{RVaR}_{\alpha,\beta}(X)$  and it is given by

$$\text{RVaR}_{\alpha,\beta}(X) = E[-X \mid -\text{VaR}_\alpha(X) \leq X \leq -\text{VaR}_\beta(X)].$$

So, in contrast to the CVaR, we only consider a specific part of the tail of the distribution of  $X$ . This makes the RVaR robust against perturbations in the underlying data.

### 3. Algorithms

In this section, we sketch the algorithms that are used to calculate the EVaR (or rather expectiles) and the RVaR. Additionally, we point out at which parts in these algorithms we apply quantum computing. Details about the used quantum techniques are given later in Section 4.

For the expectiles we perform a bisection search algorithm on a classical device and in every iteration step, the objective function is calculated on a quantum computer. This is motivated by the procedure for the VaR in Woerner and Egger (2019).

For the RVaR, we perform four operations on the quantum computer. The first two are used to obtain the VaR-values for the specified levels. The third gives us the probability to lie between these two VaR-values and the last one calculates the conditional expectation which coincides with the RVaR. This idea originates from the procedure for the CVaR in Woerner and Egger (2019).

#### 3.1. Algorithm: Expectiles

Our aim is to obtain an expectile via a root search algorithm. Note that the solution of Equation (2.1) is unique, see e.g., Bellini et al. (2014, Proposition 1). Then, for the implementation on the quantum computer we use the following equivalent representation of (2.1) in the case of  $\alpha \geq \frac{1}{2}$  with  $\beta = \frac{2\alpha-1}{1-\alpha}$ :

$$e_\alpha(X) = E[\max\{(1+\beta)X - \beta e_\alpha(X), X\}]. \quad (3.1)$$

This representation follows by using the fact that  $X = \max\{X, 0\} - \max\{-X, 0\}$ . Note, in the case of  $\alpha < \frac{1}{2}$ , we can also use the previous representation and the following methodology by using the fact that  $e_\alpha(X) = -e_{1-\alpha}(-X)$ .

Motivated by the right-hand side of the previous equation, let us introduce the fol-

lowing function for  $\alpha \geq \frac{1}{2}$ :

$$h_{X,\alpha} : \mathbb{R} \rightarrow \mathbb{R}, x \mapsto E[\max \{(1 + \beta) X - \beta x, X\}]. \quad (3.2)$$

For  $x = e_\alpha(X)$  the value of  $h_{X,\alpha}$  is equal to the right hand side in (3.1). Therefore, performing a bisection search algorithm until  $h_{X,\alpha}(x) \approx x$  gives us an approximation of the expectile  $e_\alpha(X)$ . In the end, we determine  $h_{X,\alpha}$  via a quantum algorithm.

This procedure leads to Algorithm 1. In there, we marked in red the expressions that are calculated using a quantum computer, as described in Section 4.2. In this algorithm,  $a$  and  $b$  are the minimum and maximum values of the discretized version of the random variable (compare with Section 4).  $N$  is the maximum number of iterations for the bisection search algorithm. This algorithm should stop even earlier by reaching prespecified tolerance values  $\epsilon, \delta > 0$ .

---

**Algorithm 1** Expectiles

---

```

 $x_1 \leftarrow h_{X,\alpha}(a) - a$ 
 $x_2 \leftarrow h_{X,\alpha}(b) - b$ 
for  $i = 1$  to  $N$  do
   $x \leftarrow \frac{x_1 + x_2}{2}$ 
   $y \leftarrow h_{X,\alpha}(x) - x$ 
  if  $|y| < \epsilon$  or  $|\frac{x_2 - x_1}{2}| < \delta$  then
     $e_\alpha(X) \leftarrow x$ 
    break
  end if
  if  $y > 0$  then
     $x_1 \leftarrow x$ 
  else
     $x_2 \leftarrow x$ 
  end if
end for

```

---

In order that the bisection search algorithm is well-defined, we have to check the following two properties of the map  $h_{X,\alpha}$ : First, we have to prove that it is possible to choose the starting values  $x_1$  and  $x_2$  in Algorithm 1 such that they have different signs. Second, the map  $x \mapsto h_{X,\alpha}(x) - x$  has to be continuous. For the sake of brevity, we shift these theoretical results to Appendix C.

### 3.2. Algorithm: Range Value-at-Risk

Recall that for a continuous random variable  $X$  the RVaR at levels  $\alpha$  and  $\beta$  is the following conditional expectation:

$$\text{RVaR}_{\alpha,\beta}(X) = E[-X \mid -\text{VaR}_\alpha(X) \leq X \leq -\text{VaR}_\beta(X)]. \quad (3.3)$$

We can calculate this conditional expectation directly on the quantum computer. This is illustrated by Algorithm 2. Again, we marked in red the values that are calculated via quantum computing. For  $x_1$ ,  $x_2$  and  $p$ , we use the procedures described in Woerner and Egger (2019). After the calculation of  $x_1$  and  $x_2$  we do not have to use an iterative procedure to obtain the RVaR. For the calculation of the RVaR see Section 4.3. In there, it is also explained how the probability  $p$  enters the calculation of the RVaR.

---

**Algorithm 2** Range Value-at-Risk

---

$$\begin{aligned}
x_1 &\leftarrow \text{VaR}_\alpha(X) \\
x_2 &\leftarrow \text{VaR}_\beta(X) \\
p &\leftarrow P(x_1 \leq X \leq x_2) \\
\text{RVaR}_{\alpha,\beta}(X) &\leftarrow E[-X \mid -x_1 \leq X \leq -x_2] \quad \triangleright \text{Calculation requires knowledge of } p
\end{aligned}$$


---

## 4. Implementation on a quantum computer

In this section, we describe the implementation of the operators used by a quantum algorithm to estimate the expectations in (3.2) and (3.3). The quantum algorithm that we use is the so-called amplitude estimation algorithm. In Section 4.1 we discuss important facts of different versions of amplitude estimation. Then in Sections 4.2 and 4.3 we state details for the amplitude estimation for expectiles and RVaR.

### 4.1. Quantum amplitude estimation

For a detailed introduction to quantum amplitude estimation we refer to Kaye et al. (2007, Chapter 8). We illustrate the canonical quantum circuit of amplitude estimation (QAE) in Figure 1, compare with, e.g., Brassard et al. (2000).

For the sake of convenience, we explain the idea behind QAE. To do so, assume that  $X$  is a discrete random variable attaining almost surely the values  $\{0, 1, \dots, 2^n - 1\}$ , where  $n \in \mathbb{N}$ . Further,  $X$  attains the value  $i \in \{0, 1, \dots, 2^n - 1\}$  with probability  $p_i$ . Then, we can load the distribution of  $X$  by using  $n$  qubits (analogously to bits on a classical computer) on a quantum computer. This is done by applying the following operator  $\mathcal{R}$  to the first  $n$  qubits:

$$\mathcal{R} |0\rangle_n = \sum_{i=0}^{2^n-1} \sqrt{p_i} |i\rangle_n.$$

Assuming a function  $f : \{0, 1, \dots, 2^n - 1\} \rightarrow [0, 1]$ , we can construct a new operator  $\mathcal{C}$  on the first  $n + 1$  qubits such that

$$\mathcal{C} |i\rangle_n |0\rangle = |i\rangle_n \left( \sqrt{1 - f(i)} |0\rangle + \sqrt{f(i)} |1\rangle \right).$$

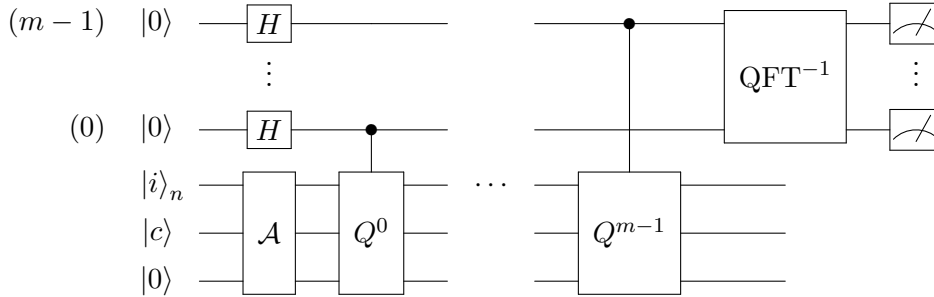


Figure 1: Quantum circuit of amplitude estimation. The distribution of  $X$  is loaded into the  $|i\rangle_n$  register, which is initially in state  $|0\rangle_n$ . Loading the distribution is part of the operator  $\mathcal{A}$ . The  $|c\rangle$  register is an ancilla qubit, initially in state  $|0\rangle$ , which is used for a comparator circuit included in  $\mathcal{A}$ . This comparator circuit is also based on  $n$  additional ancilla qubits. For the sake of brevity, we omit them here.  $H$  denotes the Hadamard gate and  $\text{QFT}^{-1}$  the inverse of the quantum Fourier transform.

By applying the operator  $\mathcal{R}$  to the first  $n$  qubits and then the operator  $\mathcal{C}$  to the first  $n + 1$  qubits, we obtain the following state

$$\sum_{i=0}^{2^n-1} \sqrt{(1-f(i))p_i} |i\rangle_n |0\rangle + \sum_{i=0}^{2^n-1} \sqrt{f(i)p_i} |i\rangle_n |1\rangle.$$

This is also the form of the state that we obtain by performing the operator  $\mathcal{A}$  in Figure 1. Now, QAE allows us to approximate the probability of the last qubit to be in state  $|1\rangle$ . This probability is given by

$$\sum_{i=0}^{2^n-1} f(i)p_i = E[f(i)].$$

Hence, by an appropriate choice of the map  $f$ , the QAE can be used to obtain estimators for the expectations in Equations (3.2) and (3.3).

The concrete forms of the operator  $\mathcal{A}$  for expectiles and RVaR are described in Sections 4.2 and 4.3. But before, we would like to mention that the quantum Fourier transform (QFT) and the controlled  $Q^j$ -gate operations (Grover operations) in Figure 1 lead to deep circuits with a high number of CNOT-gates. This circumstance is a challenging task for noisy intermediate-scale quantum devices. As a result, the design of QAE variants that achieve Grover-type speed up without the use of QFT and the series of controlled  $Q^j$ -gates has become an active area of research (Aaronson & Rall, 2019; Grinko et al., 2021; Nakaji, 2020; Suzuki et al., 2020). In addition to the canonical QAE, we also include Maximum Likelihood QAE (MLQAE) as in Suzuki et al. (2020) and Iterative QAE (IQAE) as in Grinko et al. (2021) in our analysis.

MLQAE does not use QFT and the controlled  $Q^j$ -gates. Instead, it uses different



(non-controlled) powers of  $Q$  to construct a sufficiently large sample statistic from which the desired amplitude is estimated. The repeated measurement of the state  $Q^k \mathcal{A} |0\rangle$  can be interpreted as a Bernoulli process for which the unknown hitting probability  $p_k$  can be converted into the searched amplitude. The parameters  $p_k$  are estimated for exponentially increasing powers  $k \in \{0, 2, 2^2, \dots, 2^{m-1}\}$  by the maximum likelihood method and combined to a final result.

IQAE approximates the amplitude by constructing confidence intervals that contain the target parameter with a given probability. This is done in an iterative process which reduces the length of the interval in each step until the desired approximation accuracy is achieved. As for the MLQAE, the QFT and the controlled  $Q^j$ -gates are not required. Instead, carefully chosen (non-controlled)  $Q^k$ -gates are used to construct tighter interval bounds.

We compare these variants in the case study in Section 5. Further, all variants use the same operator  $\mathcal{A}$  as input. Hence, we are allowed to restrict our attention until the end of this section to the construction of  $\mathcal{A}$ .

For the implementation on a quantum computer we assume that the support of a given random variable  $X$  is the set  $\{a, a+b, \dots, a+(2^n-1)b\}$  for some constants  $a \in \mathbb{R}$ ,  $b \in (0, \infty)$  and  $n \in \mathbb{N}$ . We describe this support by a quantum register  $|i\rangle_n$  based on  $n$  qubits. For every  $i \in \{0, \dots, 2^n-1\}$  we denote the probability that  $X$  is equal to  $a+bi$  by  $p_i$ . We define  $S := \{0, \dots, 2^n-1\}$  and fix an arbitrary point  $i^* \in S$ . Further, define the map

$$g_X : S \rightarrow \{a, a+b, \dots, a+(2^n-1)b\}, i \mapsto a+bi$$

and set  $x^* := g_X(i^*)$ .

## 4.2. Operator $\mathcal{A}$ for expectiles

In this section, we fix a level  $\frac{1}{2} \leq \alpha < 1$  and set  $\beta = \frac{2\alpha-1}{1-\alpha}$ .

To obtain the operator  $\mathcal{A}$  in Figure 1 we rewrite the integrand in (3.2) by defining the following function in dependence of  $x$ , representing a realization of  $X$ :

$$f_{x^*}(x) := \begin{cases} x & , x < x^* , \\ x + \beta x - \beta x^* & , x \geq x^* . \end{cases}$$

To obtain a map with domain  $S$  we define for each  $i \in S$ :

$$f_{i^*}(i) := (f_{x^*} \circ g_X)(i) = \begin{cases} bi + a & , i < i^* , \\ bi + a + \beta bi - \beta bi^* & , i \geq i^* . \end{cases}$$

Following the notations in Stamatopoulos et al. (2020), we set  $f_{i^*, \min} := \min_{i \in S} f_{i^*}(i)$

and  $f_{i^*,\max} := \max_{i \in S} f_{i^*}(i)$ , as well as

$$\tilde{f}_{i^*}(i) := 2 \frac{f_{i^*}(i) - f_{i^*,\min}}{f_{i^*,\max} - f_{i^*,\min}} - 1.$$

Then, for a scaling parameter  $\gamma \in [0, 1]$  we have

$$\gamma \tilde{f}_{i^*}(i) + \frac{\pi}{4} = \begin{cases} g_{i^*,0}(i) & , i < i^*, \\ g_{i^*,0}(i) + g_{i^*,1}(i) & , i \geq i^*, \end{cases}$$

with

$$g_{i^*,0}(i) := 2\gamma \left( \frac{b}{(1+\beta)b(2^n-1) - \beta b i^*} \right) i - \gamma + \frac{\pi}{4},$$

$$g_{i^*,1}(i) := 2\gamma \left( \frac{\beta b}{(1+\beta)b(2^n-1) - \beta b i^*} \right) i - 2\gamma \left( \frac{\beta b}{(1+\beta)b(2^n-1) - \beta b i^*} \right) i^*.$$

The operator  $\mathcal{A}$  is constructed in the following manner: First, load the distribution of  $X$  into the  $|i\rangle_n$  register. Secondly, perform a comparator such that the qubit  $|c\rangle$  is in state  $|1\rangle$  if  $i \geq i^*$  or  $|0\rangle$  if  $i < i^*$ . Finally, perform the multi-controlled y-rotations illustrated in Figure 2, in which a single-qubit y-rotation with respect to an angle  $\theta$  is given by the following unitary matrix:

$$R_y(\theta) := \begin{pmatrix} \cos(\theta/2) & -\sin(\theta/2) \\ \sin(\theta/2) & \cos(\theta/2) \end{pmatrix}.$$

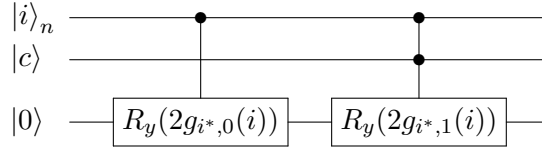


Figure 2: Circuit of multi-controlled y-rotations to describe the payoff function.

The operator  $\mathcal{A}$  maps the initial state  $|0\rangle_n |0\rangle |0\rangle$  of the  $n + 2$  qubits to the following state:

$$\sum_{i < i^*} \sqrt{p_i} |i\rangle_n |0\rangle \left( \cos(g_{i^*,0}(i)) |0\rangle + \sin(g_{i^*,0}(i)) |1\rangle \right)$$

$$+ \sum_{i \geq i^*} \sqrt{p_i} |i\rangle_n |1\rangle \left( \cos(g_{i^*,0}(i) + g_{i^*,1}(i)) |0\rangle + \sin(g_{i^*,0}(i) + g_{i^*,1}(i)) |1\rangle \right).$$

After applying the amplitude estimation to this operator we obtain an estimation of

the probability that the last qubit is in state  $|1\rangle$ . This probability is given by

$$\sum_{i < i^*} p_i \left( \sin(g_{i^*,0}(i)) \right)^2 + \sum_{i \geq i^*} p_i \left( \sin(g_{i^*,0}(i) + g_{i^*,1}(i)) \right)^2.$$

Applying the approximation

$$\left( \sin \left( \gamma \tilde{f}_{i^*}(i) + \frac{\pi}{4} \right) \right)^2 \approx \gamma \tilde{f}_{i^*}(i) + \frac{1}{2},$$

to this probability, we obtain an estimator for an affine transformation of  $h_{X,\alpha}(x)$ .

**Example 4.1** (Normal distribution). We assume a normal distributed random variable  $Y$  with mean  $\mu \in \mathbb{R}$  and standard deviation  $\sigma \in (0, \infty)$ . We denote by  $\varphi$ , respectively  $\Phi$ , the probability density function, respectively the cumulative distribution function, of a standard normal distributed random variable. For each  $y \in \mathbb{R}$  it holds that

$$h_{Y,\alpha}(y) = \mu + \beta \left( 1 - \Phi \left( \frac{y - \mu}{\sigma} \right) \right) (\mu - y) + \beta \sigma \varphi \left( \frac{y - \mu}{\sigma} \right).$$

To obtain an estimator for this expression we use a random variable  $X$  with support given by  $\left\{ \mu - 3\sigma, \mu - 3\sigma + \frac{6\sigma}{2^n - 1}, \dots, \mu + 3\sigma \right\}$  and probabilities obtained from the distribution of  $Y$ . The function  $f_{i^*}$  is defined by the parameters  $a = \mu - 3\sigma$  and  $b = \frac{6\sigma}{2^n - 1}$ . Hence, it holds that

$$\begin{aligned} f_{i^*,\min} &= \mu - 3\sigma, \\ f_{i^*,\max} &= \mu + 3\sigma + 6\beta\sigma \left( 1 - \frac{i^*}{2^n - 1} \right). \end{aligned}$$

This leads to the following values for the multi-controlled  $y$ -rotations:

$$\begin{aligned} g_{i^*,0}(i) &= 2\gamma \left( \frac{1}{(1 + \beta)(2^n - 1) - \beta i^*} \right) i - \gamma + \frac{\pi}{4}, \\ g_{i^*,1}(i) &= 2\gamma \left( \frac{\beta}{(1 + \beta)(2^n - 1) - \beta i^*} \right) i - 2\gamma \left( \frac{\beta}{(1 + \beta)(2^n - 1) - \beta i^*} \right) i^*. \end{aligned}$$

### 4.3. Operator $\mathcal{A}$ for Range Value-at-Risk

The basic idea for calculating the RVaR is to combine two comparator circuits and use them to control the application of an appropriate  $y$ -rotation similar to the one in Figure 2. This is then combined with the calculation of VaR-values as shown in Algorithm 2.

To define the  $y$ -rotation we proceed analogously to Section 4.2. Given the affine

mapping  $g := g_X$  with  $g_{\min} := \min_{i \in S} g(i)$  and  $g_{\max} := \max_{i \in S} g(i)$ , we define

$$\tilde{g}(i) := 2 \frac{g(i) - g_{\min}}{g_{\max} - g_{\min}} - 1.$$

For the scaling parameter  $\gamma \in [0, 1]$  we set

$$\hat{g}(i) := \gamma \tilde{g}(i) + \frac{\pi}{4}.$$

The  $y$ -rotations are then given by  $R_y(2\hat{g}(i))$ .

To explain the simultaneous application of two different comparators in more detail, we extend the notations from Section 4.2. For  $k \in \mathbb{Z}$ , let  $\text{cmp}_1(k)$  and  $\text{cmp}_2(k)$  be the unitary operators defined by the following rule:

$$\begin{aligned} \text{cmp}_1(k) : |i\rangle_n |0\rangle &\mapsto \begin{cases} |i\rangle_n |1\rangle & , i \geq k, \\ |i\rangle_n |0\rangle & , i < k, \end{cases} \\ \text{cmp}_2(k) : |i\rangle_n |0\rangle &\mapsto \begin{cases} |i\rangle_n |1\rangle & , i < k, \\ |i\rangle_n |0\rangle & , i \geq k. \end{cases} \end{aligned}$$

These comparator circuits use the same  $n$ -qubit register  $|i\rangle_n$  to store the binary representation of  $i$ . Further, comparator circuit  $j$  uses an  $(n-1)$ -qubit register  $|a_j\rangle$  for ancillas and one qubit  $|t_j\rangle$  to save the result of the comparison, see Figure 3.

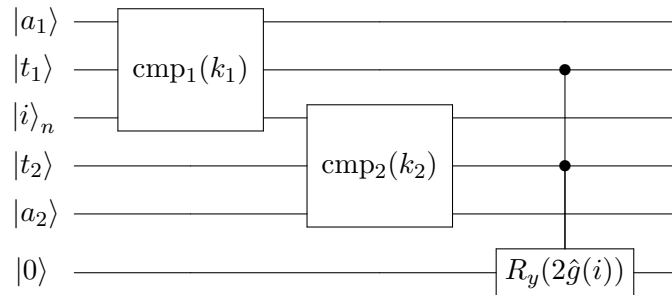


Figure 3: Quantum circuit for calculating  $\text{RVaR}_{\alpha, \beta}(X)$ . The distribution of  $X$  is loaded into  $|i\rangle_n$ . The ancillas for the comparator circuits are stored in  $|a_1\rangle$  and  $|a_2\rangle$ . Comparator results are placed in  $|t_1\rangle$  and  $|t_2\rangle$ , which are used to control the  $y$ -rotation  $R_y(2\hat{g}(i))$ .

We combine the two comparator circuits in the sense that they constrain  $i$  from both sides and the two result qubits control the  $y$ -rotation. Finally, the operator  $\mathcal{A}$  is created by loading the distribution into the qubit register  $|i\rangle_n$ . Note that at this point  $\mathcal{A}$  still depends on the choice of  $k_1$  and  $k_2$ .

Suppose  $k_2 < k_1$ . If we neglect the ancillas and apply  $\mathcal{A}$  to the initial state  $|0\rangle_n |0\rangle |0\rangle |0\rangle$ ,

where the second and third qubit represent  $t_1$  and  $t_2$ , we obtain

$$\begin{aligned} \mathcal{A} |0\rangle_n |0\rangle |0\rangle |0\rangle &= \sum_{i=0}^{k_2-1} \sqrt{p_i} |i\rangle_n |1\rangle |0\rangle |0\rangle \\ &+ \sum_{i=k_2}^{k_1} \sqrt{p_i} |i\rangle_n |1\rangle |1\rangle \left( \cos(\hat{g}(i)) |0\rangle + \sin(\hat{g}(i)) |1\rangle \right) \\ &+ \sum_{i=k_1+1}^{2^n-1} \sqrt{p_i} |i\rangle_n |0\rangle |1\rangle |0\rangle. \end{aligned}$$

The probability that this state is  $|1\rangle$  at the position of the last qubit is

$$\sum_{i=k_2}^{k_1} p_i \sin^2(\hat{g}(i)).$$

If we apply the approximation  $\sin^2(\hat{g}(i)) \approx \gamma \tilde{g}(i) + \frac{\pi}{4}$  as in Section 4.2 and choose for  $k_1$  and  $k_2$  integer approximations for  $\text{VaR}_\alpha(g^{-1} \circ X)$  and  $\text{VaR}_\beta(g^{-1} \circ X)$ , then we obtain

$$\sum_{i=k_2}^{k_1} p_i \sin^2(\hat{g}(i)) \approx \frac{-2\gamma P(k_2 \leq X \leq k_1) \text{RVaR}_{\alpha,\beta}(g^{-1} \circ X) - g_{\min}}{g_{\max} - g_{\min}} - \gamma + \frac{1}{2}.$$

From this expression we can reconstruct  $\text{RVaR}_{\alpha,\beta}(X)$ . Note that integer approximations for  $\text{VaR}_\alpha(g^{-1} \circ X)$  and  $\text{VaR}_\beta(g^{-1} \circ X)$  and an estimate for  $P(k_2 \leq X \leq k_1)$  can be obtained with the quantum methods in Woerner and Egger (2019).

## 5. Case study

We denote by  $N(\mu, \sigma)$  a normal distribution with mean  $\mu$  and standard deviation  $\sigma$ . By  $LN(\mu, \sigma)$  we denote a lognormal distribution with expectation  $\exp\left(\mu + \frac{\sigma^2}{2}\right)$ . Finally,  $\Gamma(p, q)$  denotes a gamma distribution with mean  $p/q$ .

In this section, we analyze the computation of VaR, ES, expectiles and RVaR on the IBMQ Kolkata quantum device. All computations are performed with the help of the qiskit framework, see (Treinish et al., 2022). To keep the explanations in this section as short as possible, we shifted additional information about the methods to optimize our calculations to Appendix A.

We calculate the risk measures for normal, lognormal and gamma distributions, because of their popularity in different disciplines. For instance, the lognormal distribution is applied in the description of growth processes (Huxley, 1993; Sutton, 1997) as well as for modeling stock prices in the Black-Scholes model (Black & Scholes, 1973). The gamma distribution is widely used in actuarial science to model the claim size distribution for non-life insurance contracts (Boland, 2007; Laudag e et al., 2019; Ohlsson & Johansson, 2010). It is also applied for failure-time analysis (Scheiner & Gurevitch,

2001).

Our analysis is based on Example 4.1. As in there, let  $Y$  denote a continuously distributed random variable with density function  $f$ . As a first step, we would like to express the values of  $f$  as norm-squared amplitudes of a suitable quantum state. Given that we have  $n$  qubits available, we need to restrict our attention to a bounded interval included in the domain of  $f$  and discretize this interval by  $2^n$  points. Formally, we move from the continuous random variable  $Y$  to a discretized version of it, denoted by  $X$ . That means also that we replace  $f$  with the density function of  $X$ . The quantum state will then capture the probabilities of  $g_X^{-1} \circ X$ , where  $g_X$  is the affine mapping that transforms  $\{0, 1, \dots, N - 1\}$  to the support of  $X$ . Table 1 summarizes the parameters for the distributions of  $-Y$  (normal, lognormal, gamma) and the interval to which the associated density function is restricted. The use of different intervals on the simulator and the real hardware stems from the consideration of different levels.

Table 1: Parameters of the applied distributions and the intervals for their discretization.

Distribution of $-Y$	Parameters	Interval simulator	Interval real hardware
Normal $N(\mu, \sigma^2)$	$\mu = 3, \sigma = 1$	[0, 10]	[0, 6]
Lognormal $LN(\mu, \sigma^2)$	$\mu = 0, \sigma = \frac{1}{2}$	[0, 10]	[0, 3]
Gamma $\Gamma(p, q)$	$p = 1, q = 1$	[0, 10]	[0, 3]

There are two effects that have a major impact on the quality of the calculation of risk measures on a quantum computer. One is the coherence time and gate fidelity, i.e., the computational accuracy of the quantum computer. The other is the accuracy of the approximation of the continuous density function  $f$  by the probability mass function of  $g_X^{-1} \circ X$ .

The latter depends on the number of qubits for loading the distribution, because it determines the granularity of the discretization of the domain of  $f$ . Figure 4 shows the influence of hardware noise and qubit count on the distribution. We see that hardware noise leads to inaccuracies in the description of the density function. This is typical for noisy intermediate-scale quantum devices.

The granularity of the discretization is of particular interest for the calculation of risk measures, because it can lead to noticeable changes in the capital requirements. To illustrate this statement, we compare the results between the true value of a risk measure and its value calculated on a quantum simulator in Figure 5. This shows that good results are produced even for levels in the range of  $\lambda = \alpha = 0.05$  and  $\beta = 0.005$  if the number of qubits is sufficiently large. For all risk measures, the approximation error (relative to the length of the interval to discretize the domain of the density function) converges sufficiently fast towards zero if the number of qubits for loading the distribution increases.

It is worth noting that the parameter  $\gamma$ , which appears in the construction of the operator  $\mathcal{A}$ , has a significant impact on the accuracy of results. In general, a suitable choice for  $\gamma$  depends on the distribution and the risk measure under consideration. As a rule of thumb, we recommend a value of  $\gamma \approx \pi/8$  for VaR and CVaR, and a value of

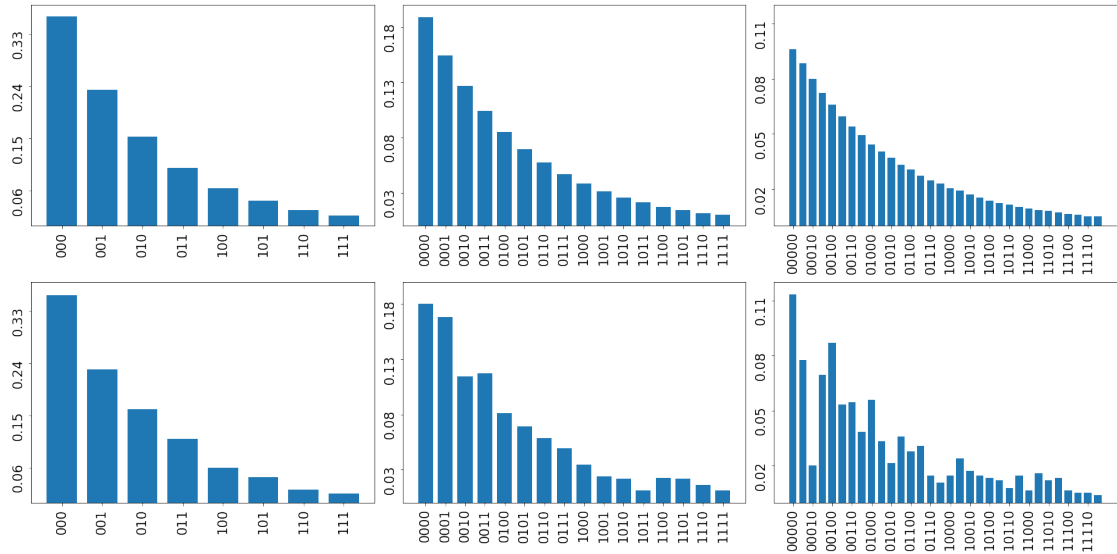


Figure 4: Distribution loading for the gamma distribution  $\Gamma(1, 1)$  with respect to different numbers of qubits. The blue bars describe the quantum state generated by the distribution circuit, or equivalently, the probability mass function of  $g_X^{-1} \circ X$ . The first row shows the results of a noiseless simulator, the second row the results of the quantum computer. From the left to the right column, the number of qubits is 3, 4 and 5.

$\gamma \approx \pi/4$  for RVaR and expectile.

Besides the distribution loading, the number of qubits is also responsible for the approximation accuracy in the canonical QAE, because it determines the amount of classical bits used to approximate the result. Figure 6 shows in the case of an expectile, how an increase in the number of ancilla qubits (parameter  $m$  in Figure 1) allows for an improvement in the accuracy of results. This plot is motivated by Figure 4 in Woerner and Egger (2019).

Figure 7 illustrates the performance of our algorithms on a real quantum device. Due to the existing hardware limitations, we have to restrict ourselves to three qubits when loading the distribution on a real quantum computer. Accordingly, we choose levels  $\lambda = \alpha = 0.20$  and  $\beta = 0.05$ . Also, we restrict ourselves to  $m = 3$  qubits for the canonical QAE. Table 2 gives an overview of the number of qubits and CNOT-gates that were used in the procedure. The algorithms are run with different numbers of shots to test potential improvements in accuracy for IQAE and MLQAE. In general, the accuracy of the canonical QAE does not change with an increased number of shots, because the canonical QAE leads to the most frequent result. This value does not change with an increasing number of shots in general, compare with the third column in Figure 7.

First, we note that the accuracy for VaR and expectiles is substantially higher than for CVaR and RVaR. This stems from the usage of a bisection search algorithm for VaR and expectiles. VaR and expectiles are not direct results of the outcome of the amplitude

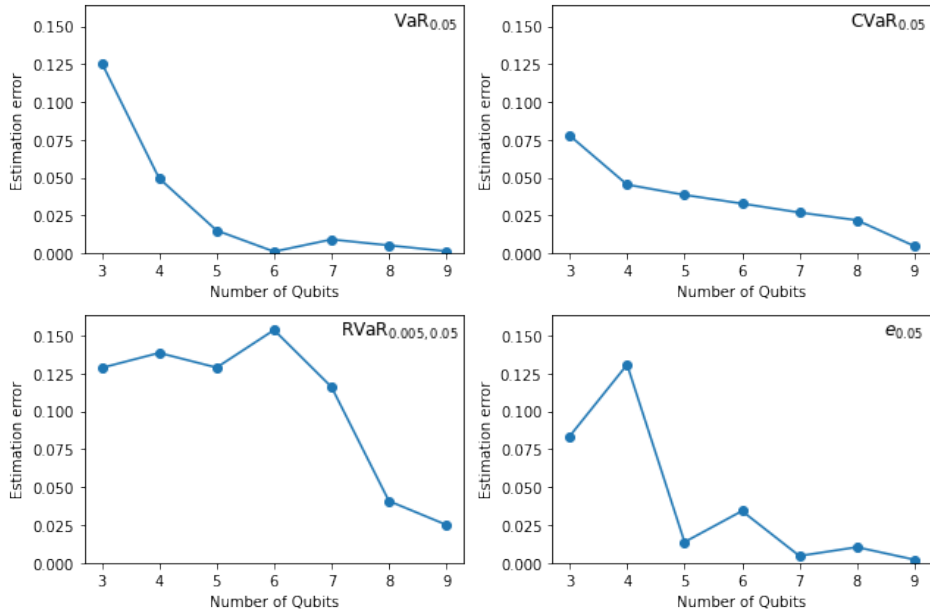


Figure 5: The estimation error on a simulator as a function of the number of qubits used for loading the distribution. The error is given relatively to the length of the domain on which  $f$  is defined. For the results of this plot we applied the IQAE with target precision 0.05 and confidence level 0.01 to  $\Gamma(1, 1)$ . We used  $\gamma = \pi/8$  for VaR and CVaR and  $\gamma = \pi/4$  for RVaR and expectile. An analogous error behavior is also given for other distributions (see Appendix B).

Table 2: The number of qubits (NoQ) and CNOTs used in the calculation of risk measures with respect to  $\Gamma(1, 1)$ . For the results with respect to other distributions we refer to Appendix B.

Algorithm	VaR <sub><math>\lambda</math></sub> ( $X$ )		CVaR <sub><math>\lambda</math></sub> ( $X$ )		RVaR <sub><math>\alpha, \beta</math></sub> ( $X$ )		e <sub><math>\alpha</math></sub> ( $X$ )	
	NoQ	CNOTs	NoQ	CNOTs	NoQ	CNOTs	NoQ	CNOTs
IQAE	6	7.568	7	13.482	10	73.916	7	20.481
MLQAE	6	2.602	7	5.525	10	27.783	7	5.847
Canonical QAE	9	15.506	10	33.752	13	194.447	10	35.962

estimation. The latter is only used to select the next subinterval in the bisection search algorithm. This selection is robust to inaccuracies introduced by the quantum hardware. Thus, if the true value is contained in the interval representing the domain of  $f$ , then the bisection search algorithm leads in most cases to a tighter interval that contains the true value. The main influence on the estimation error (if the tolerance values  $\epsilon, \delta$  in Algorithm 1 are small enough) stems from the discretization of the domain of  $f$ , i.e., in the majority of cases the estimated value is the closest possible to the true value regarding the chosen discretization. In this sense, the algorithms for VaR and expectiles



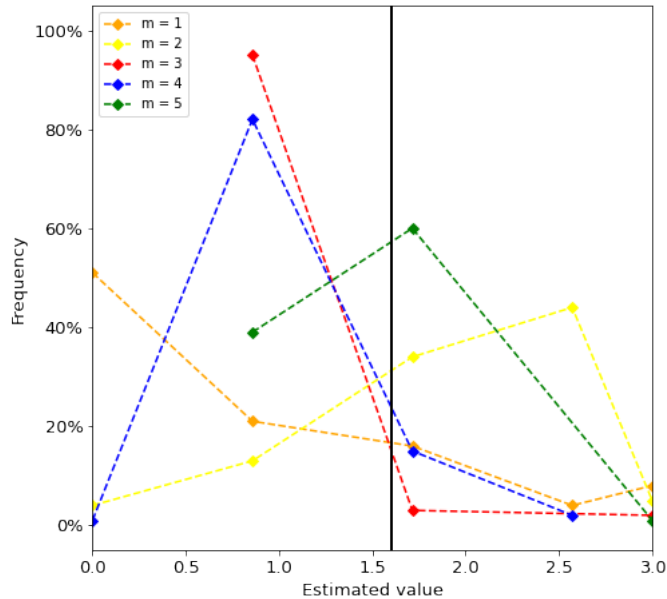


Figure 6: Estimation for the expectile calculated with the canonical QAE on a simulator. We used  $\gamma = \pi/4$ . The underlying distribution is  $\Gamma(1, 1)$ . The exact value is indicated by the black line. With an increased number of ancilla qubits  $m$ , the most frequent result approaches the exact value. An analogous error behavior is also given for other distributions (see Appendix B).

converge towards the exact results and hence, they are robust against the noise in the quantum hardware.

In contrast, the CVaR and the RVaR are direct results of the amplitude estimation by relying on the conditional probability measure. The QAE result enters the denominator of the conditional probability and is usually close to zero. Thus, the result is very sensitive to inaccuracies in the calculation on real hardware, which explains the high deviations in Figure 7. This effect does not appear so strongly for the canonical amplitude estimation, because the solutions are restricted to the set  $\{\sin(\pi y/2^m) \mid y \in \{0, \dots, 2^{m-1}\}\}$ . Thus, for fixed  $m$ , the denominator of the conditional probability does not become arbitrarily small when using canonical QAE.

For  $\text{RVaR}_{\alpha, \beta}(X)$  we find that the estimation error for  $LN(0, 1/2)$  and  $\Gamma(1, 1)$  is in most of the cases larger than for  $N(3, 1)$ . Compared to the normal distribution, the lognormal and the gamma distribution admit heavier tails. Hence,  $\text{VaR}_{\alpha}(X)$  and  $\text{VaR}_{\beta}(X)$  are close to each other. The aforementioned effect applies significantly.

Finally, we would like to mention that for the given hardware constraints, IQAE yields slightly better results than MLQAE when considering VaR and expectile, whereas MLQAE appears more robust when applied to CVaR and RVaR.

Summarizing, the results for CVaR and RVaR are affected by the noise on the quan-

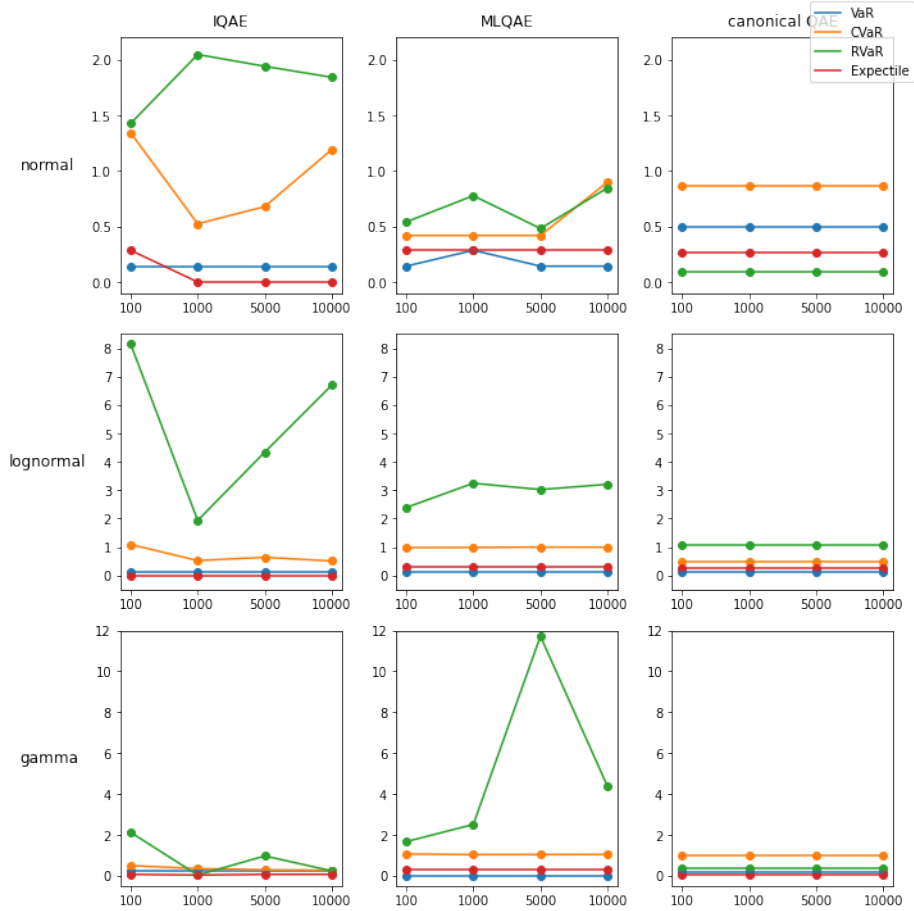


Figure 7: The estimation error on the IBMQ Kolkata quantum device as a function of the number of shots. The error is given relatively to the length of the interval for discretizing the domain of  $f$ . IQAE was applied with a confidence level of 0.05, MLQAE with a evaluation schedule of 3 and canonical QAE with  $m = 3$ . Unlike RVaR, the expectile calculations, with the chosen algorithms and with 3 qubits for the distribution, are sufficiently reliable on a real hardware.

tum hardware. Instead, in the case of calculating VaR and expectiles, this noise is compensated by the bisection search algorithm and the estimated values are close to the exact values.

## 6. Conclusion

We present two quantum-based algorithms to calculate expectiles and Range Value-at-Risk. These algorithms are based on quantum amplitude estimation. A bisection search algorithm is performed on a classical computer to calculate expectiles. The objective function is evaluated by amplitude estimation on a quantum device. This is in line with

the idea to calculate the Value-at-Risk as described in Woerner and Egger (2019). On the other hand, the Range Value-at-Risk is a direct outcome of the amplitude estimation. The methodology is inspired by the calculation of the Conditional Value-at-Risk in Woerner and Egger (2019).

By a case study, we find that the algorithms converge sufficiently fast on a simulator towards the true values, if the number of qubits to load the distribution is increased. The lowest estimation errors on the IBMQ Kolkata device are obtained for the expectile by the IQAE method and for RVaR by the MLQAE method. The calculation of expectiles turns out to be robust against noises on the real hardware. On the other hand, the Range Value-at-Risk is significantly affected by this noise.

This paper is a next step to calculate risk measures via quantum computing. Risk measures that are not considered in this manuscript can be of interest for future research. For example, expectiles are special cases of so-called shortfall risk measures, see e.g., Föllmer and Schied (2016). Also other utility based risk measures could be analyzed, like e.g., the optimized certainty equivalent (Ben-Tal & Teboulle, 1986, 2007) or the optimal expected utility risk measure (Geissel et al., 2018; Vinel & Krokmal, 2017).

## References

- Aaronson, S., & Rall, P. (2019, December). Quantum Approximate Counting, Simplified. In *Symposium on Simplicity in Algorithms (SOSA)* (pp. 24–32). Society for Industrial; Applied Mathematics. <https://doi.org/10.1137/1.9781611976014.5>
- Bellini, F., & Di Bernardino, E. (2017). Risk management with expectiles. *The European Journal of Finance*, 23(6), 487–506. <https://doi.org/10.1080/1351847X.2015.1052150>
- Bellini, F., Klar, B., Müller, A., & Rosazza Gianin, E. (2014). Generalized quantiles as risk measures. *Insurance: Mathematics and Economics*, 54, 41–48. <https://doi.org/10.1016/j.insmatheco.2013.10.015>
- Ben-Tal, A., & Teboulle, M. (1986). Expected Utility, Penalty Functions, and Duality in Stochastic Nonlinear Programming. *Management Science*, 32(11), 1445–1466. <https://doi.org/10.1287/mnsc.32.11.1445>
- Ben-Tal, A., & Teboulle, M. (2007). An Old-New Concept of Convex Risk Measures: The Optimized Certainty Equivalent. *Mathematical Finance*, 17(3), 449–476. <https://doi.org/10.1111/j.1467-9965.2007.00311.x>
- Black, F., & Scholes, M. (1973). The Pricing of Options and Corporate Liabilities. *Journal of Political Economy*, 81(3), 637–654. Retrieved October 26, 2022, from <https://www.jstor.org/stable/1831029>
- Boland, P. J. (2007, March). *Statistical and Probabilistic Methods in Actuarial Science*. Chapman; Hall/CRC. <https://doi.org/10.1201/9781584886969>
- Bonnet, É., Miltzow, T., & Rzażewski, P. (2018). Complexity of Token Swapping and Its Variants. *Algorithmica*, 80(9), 2656–2682. <https://doi.org/10.1007/s00453-017-0387-0>

- Brassard, G., Hoyer, P., Mosca, M., & Tapp, A. (2000). Quantum Amplitude Amplification and Estimation. *AMS Contemporary Mathematics Series*, 305. <https://doi.org/10.1090/conm/305/05215>
- Chakrabarti, S., Krishnakumar, R., Mazzola, G., Stamatopoulos, N., Woerner, S., & Zeng, W. J. (2021). A Threshold for Quantum Advantage in Derivative Pricing. *Quantum*, 5, 463. <https://doi.org/10.22331/q-2021-06-01-463>
- Cheridito, P., & Li, T. (2009). Risk Measures on Orlicz Hearts. *Mathematical Finance*, 19(2), 189–214. <https://doi.org/10.1111/j.1467-9965.2009.00364.x>
- Cont, R., Deguest, R., & Scandolo, G. (2010). Robustness and sensitivity analysis of risk measurement procedures. *Quantitative Finance*, 10(6), 593–606. <https://doi.org/10.1080/14697681003685597>
- Cowtan, A., Dilkes, S., Duncan, R., Krajenbrink, A., Simmons, W., & Sivarajah, S. (2019). On the Qubit Routing Problem. In W. v. Dam & L. Mancinska (Eds.), *14th Conference on the Theory of Quantum Computation, Communication and Cryptography (TQC 2019)* (5:1–5:32, Vol. 135). Schloss Dagstuhl–Leibniz-Zentrum fuer Informatik. <https://doi.org/10.4230/LIPIcs.TQC.2019.5>
- Egger, D. J., Gambella, C., Marecek, J., McFaddin, S., Mevissen, M., Raymond, R., Simonetto, A., Woerner, S., & Yndurain, E. (2020). Quantum Computing for Finance: State-of-the-Art and Future Prospects. *IEEE Transactions on Quantum Engineering*, 1, 1–24. <https://doi.org/10.1109/TQE.2020.3030314>
- Egger, D. J., Gutiérrez, R. G., Mestre, J. C., & Woerner, S. (2021). Credit Risk Analysis Using Quantum Computers. *IEEE Transactions on Computers*, 70(12), 2136–2145. <https://doi.org/10.1109/TC.2020.3038063>
- Embrechts, P., Liu, H., Mao, T., & Wang, R. (2020). Quantile-based risk sharing with heterogeneous beliefs. *Mathematical Programming*, 181(2), 319–347. <https://doi.org/10.1007/s10107-018-1313-1>
- Fissler, T., & Ziegel, J. F. (2021). On the elicibility of range value at risk. *Statistics & Risk Modeling*, 38(1-2), 25–46. <https://doi.org/10.1515/strm-2020-0037>
- Föllmer, H., & Schied, A. (2016, July). *Stochastic Finance: An Introduction in Discrete Time*. De Gruyter. <https://doi.org/10.1515/9783110463453>
- Geissel, S., Sass, J., & Seifried, F. T. (2018). Optimal expected utility risk measures. *Statistics & Risk Modeling*, 35(1-2), 73–87. <https://doi.org/10.1515/strm-2017-0027>
- Grinko, D., Gacon, J., Zoufal, C., & Woerner, S. (2021). Iterative quantum amplitude estimation. *npj Quantum Information*, 7(1), 1–6. <https://doi.org/10.1038/s41534-021-00379-1>
- Huxley, J. S. (1993, October). *Problems of Relative Growth*. Johns Hopkins University Press.
- Kaye, P., Laflamme, R., & Mosca, M. (2007). *An introduction to quantum computing*. Oxford Univ. Press.
- Koch-Medina, P., & Munari, C. (2022). Qualitative robustness of utility-based risk measures. *Annals of Operations Research*. <https://doi.org/10.1007/s10479-022-04885-z>

- Krätschmer, V., Schied, A., & Zähle, H. (2014). Comparative and qualitative robustness for law-invariant risk measures. *Finance and Stochastics*, 18(2), 271–295. <https://doi.org/10.1007/s00780-013-0225-4>
- Laudagé, C., Desmettre, S., & Wenzel, J. (2019). Severity modeling of extreme insurance claims for tariffication. *Insurance: Mathematics and Economics*, 88, 77–92. <https://doi.org/10.1016/j.insmatheco.2019.06.002>
- Li, G., Ding, Y., & Xie, Y. (2019). Tackling the Qubit Mapping Problem for NISQ-Era Quantum Devices. *Proceedings of the Twenty-Fourth International Conference on Architectural Support for Programming Languages and Operating Systems*, 1001–1014. <https://doi.org/10.1145/3297858.3304023>
- Mapomatic. (2022, October). Retrieved October 26, 2022, from <https://github.com/Qiskit-Partners/mapomatic>
- Nakaji, K. (2020). Faster amplitude estimation. *Quantum Information and Computation*, 20(13&14), 1109–1123. <https://doi.org/10.26421/QIC20.13-14-2>
- Nation, P. D., Kang, H., Sundaresan, N., & Gambetta, J. M. (2021). Scalable Mitigation of Measurement Errors on Quantum Computers. *PRX Quantum*, 2(4), 040326. <https://doi.org/10.1103/PRXQuantum.2.040326>
- Newey, W. K., & Powell, J. L. (1987). Asymmetric Least Squares Estimation and Testing. *Econometrica*, 55(4), 819–847. <https://doi.org/10.2307/1911031>
- Ohlsson, E., & Johansson, B. (2010). *Non-Life Insurance Pricing with Generalized Linear Models*. Springer. <https://doi.org/10.1007/978-3-642-10791-7>
- Scheiner, S. M., & Gurevitch, J. (2001, April). *Design and Analysis of Ecological Experiments*. Oxford University Press.
- Stamatopoulos, N., Egger, D. J., Sun, Y., Zoufal, C., Iten, R., Shen, N., & Woerner, S. (2020). Option Pricing using Quantum Computers. *Quantum*, 4, 291. <https://doi.org/10.22331/q-2020-07-06-291>
- Stamatopoulos, N., Mazzola, G., Woerner, S., & Zeng, W. J. (2022). Towards Quantum Advantage in Financial Market Risk using Quantum Gradient Algorithms. *Quantum*, 6, 770. <https://doi.org/10.22331/q-2022-07-20-770>
- Sutton, J. (1997). Gibrat’s Legacy. *Journal of Economic Literature*, 35(1), 40–59. Retrieved October 26, 2022, from <https://www.jstor.org/stable/2729692>
- Suzuki, Y., Uno, S., Raymond, R., Tanaka, T., Onodera, T., & Yamamoto, N. (2020). Amplitude estimation without phase estimation. *Quantum Information Processing*, 19(2), 75. <https://doi.org/10.1007/s11128-019-2565-2>
- Treinish, M., Gambetta, J., Nation, P., qiskit-bot, Kassebaum, P., Rodríguez, D. M., González, S. d. l. P., Hu, S., Lishman, J., Krsulich, K., Garrison, J., Yu, J., Bello, L., Marques, M., Gacon, J., McKay, D., Gomez, J., Capelluto, L., Travis-S-IBM, . . . Glen. (2022, October). Qiskit/qiskit: Qiskit 0.39.0. <https://doi.org/10.5281/zenodo.7195914>
- Vinel, A., & Krokhmal, P. A. (2017). Certainty equivalent measures of risk. *Annals of Operations Research*, 249(1), 75–95. <https://doi.org/10.1007/s10479-015-1801-0>
- Woerner, S., & Egger, D. J. (2019). Quantum risk analysis. *npj Quantum Information*, 5(1), 1–8. <https://doi.org/10.1038/s41534-019-0130-6>

## A. Technical facts

In the following, we give details about the improvements of the hardware calculations in Section 5. There exist four possibilities for a software user to influence the performance on a real quantum device. We discuss them in the following:

1. *Transpilation of circuits.* IBMQ Kolkata can only run a small set of five gates. These five gates are universal in the sense that any circuit can be decomposed into them. The decomposition of a circuit into these five gates is not unique. Thus, there are several decompositions, which generally have significant performance differences.
2. *Routing problem.* Only a subset of the totally available qubits is needed for the calculation. So, we have the freedom to choose between subsets with different connectivity properties. Connectivity determines how many SWAP gates must be added to allow any communication between non-adjacent qubits to be performed. Finding an optimal routing in terms of CNOT-depth and CNOT-count is highly nontrivial and known to be at least NP-hard (Bonnet et al., 2018; Cowtan et al., 2019). Since routing and transpiling affect each other, they are usually optimized simultaneously. We used the SWAP-based bidirectional heuristic search algorithm (SABRE, (Li et al., 2019)) for the simultaneous optimization (qiskit optimization level 3). We executed it several times to stabilize our results.
3. *Coherence time and gate fidelity.* With fixed routing, there are usually several subsets of qubits that satisfy the exact same connectivity properties. Ideally, the subset with the best parameters in terms of computational quality is selected. We evaluated the computational quality using the Mapomatic (“mapomatic”, 2022) package.
4. *Post-processing.* We have used post-measurement-error-mitigation included in the package M3 (Nation et al., 2021).

## B. Figures and tables

The figures show the convergence behavior on a simulator and the number of CNOTs used on a real quantum computer with respect to the lognormal and the normal distribution.

Table 3: The number of qubits (NoQ) and CNOTs used in the calculation of risk measures with respect to  $LN(0, 1/2)$ .

Algorithm	$\text{VaR}_\lambda(X)$		$\text{CVaR}_\lambda(X)$		$\text{RVaR}_{\alpha,\beta}(X)$		$e_\alpha(X)$	
	NoQ	CNOTs	NoQ	CNOTs	NoQ	CNOTs	NoQ	CNOTs
IQAE	6	8.193	7	15.246	10	107.038	7	16.581
MLQAE	6	2.565	7	5.485	10	29.578	7	5.946
Canonical QAE	9	15.509	10	33.541	13	192.451	10	35.528

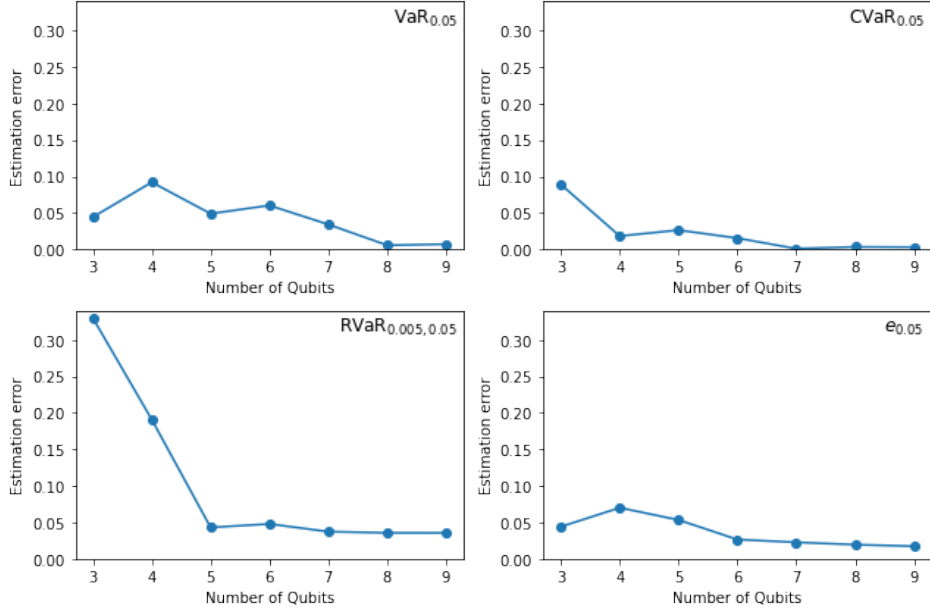


Figure 8: The estimation error on a simulator as a function of the number of qubits used for loading the distribution. The error is given relatively to the length of the domain on which  $f$  is defined. For the results of this plot we applied the IQAE with target precision 0.05 and confidence level 0.01 to  $LN(0, 1/2)$ . We used  $\gamma = \pi/8$  for VaR and CVaR and  $\gamma = \pi/4$  for RVaR and expectile.

Table 4: The number of qubits (NoQ) and CNOTs used in the calculation of risk measures with respect to  $N(3, 1)$ .

Algorithm	VaR <sub><math>\lambda</math></sub> ( $X$ )		CVaR <sub><math>\lambda</math></sub> ( $X$ )		RVaR <sub><math>\alpha, \beta</math></sub> ( $X$ )		e <sub><math>\alpha</math></sub> ( $X$ )	
	NoQ	CNOTs	NoQ	CNOTs	NoQ	CNOTs	NoQ	CNOTs
IQAE	6	7.957	7	14.216	10	109.872	7	23.330
MLQAE	6	2.758	7	5.178	10	26.461	7	5.494
Canonical QAE	9	15.506	10	33.752	13	194.447	10	34.945

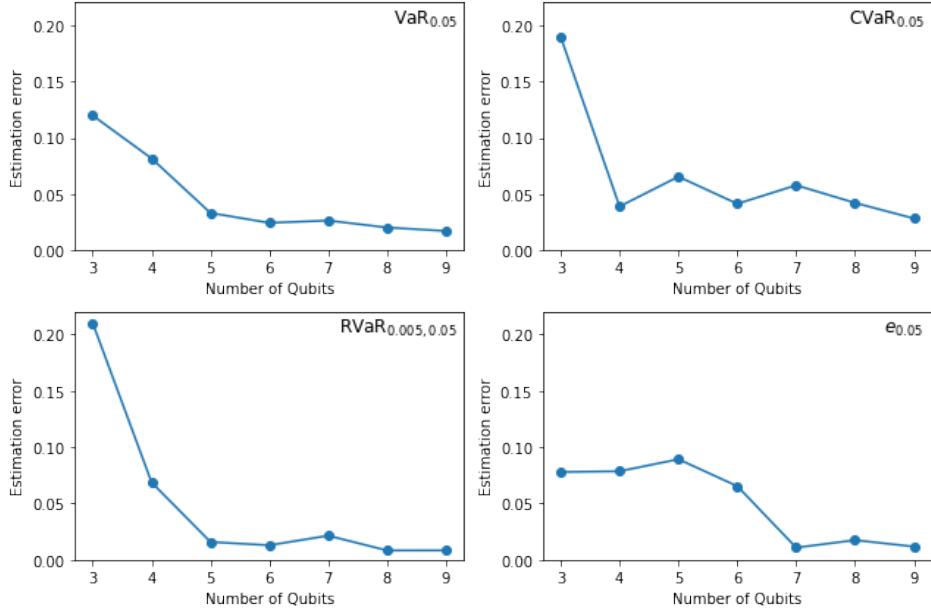


Figure 9: The estimation error on a simulator as a function of the number of qubits used for loading the distribution. The error is given relatively to the length of the domain on which  $f$  is defined. For the results of this plot we applied the IQAE with target precision 0.05 and confidence level 0.01 to  $LN(3,0)$ . We used  $\gamma = \pi/8$  for VaR and CVaR and  $\gamma = \pi/4$  for RVaR and expectile.



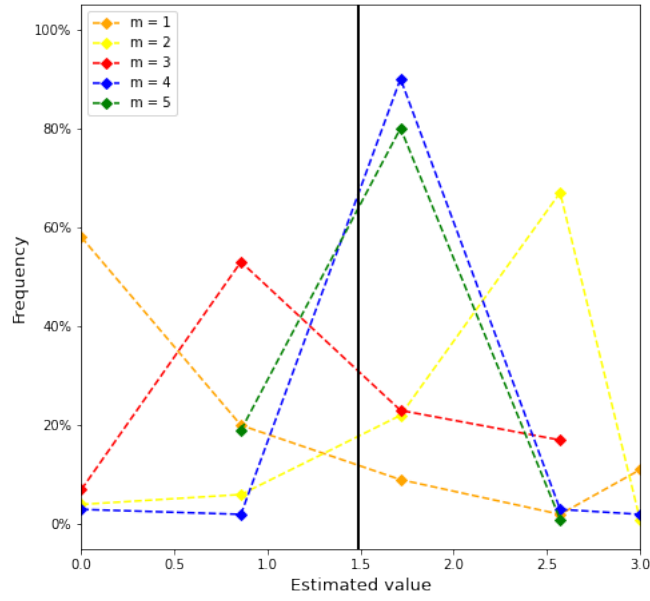


Figure 10: Estimation for the expectile calculated with the canonical QAE on a simulator. We used  $\gamma = \pi/4$ . The underlying distribution is  $LN(0, 1/2)$ . The exact value is indicated by the black line. With an increased number of ancilla qubits  $m$ , the most frequent result approaches the exact value.

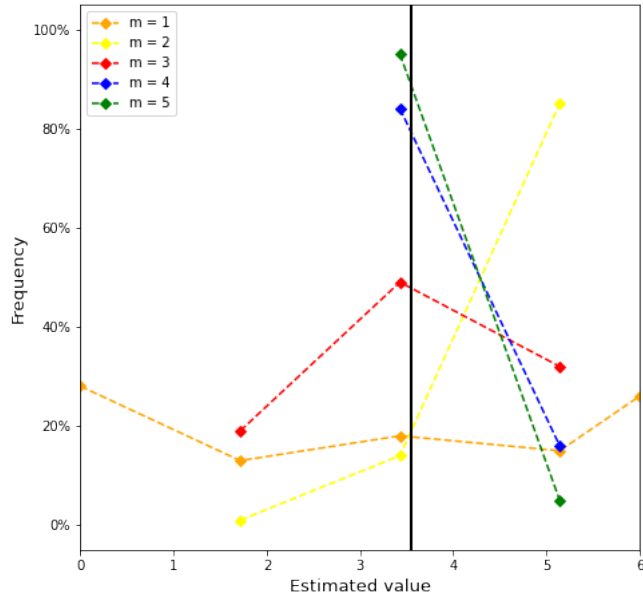


Figure 11: Estimation for the expectile calculated with the canonical QAE on a simulator. We used  $\gamma = \pi/4$ . The underlying distribution is  $N(3, 1)$ . The exact value is indicated by the black line. With an increased number of ancilla qubits  $m$ , the most frequent result approaches the exact value.

## C. Risk measures: Mathematical background

We recall some mathematical background of risk measures. In particular, we state the definition of a general risk measure and give further properties of expectiles that are important for the applicability of the bisection search algorithm in Section 3.1.

To do so, we assume an atomless probability space  $(\Omega, \mathcal{F}, P)$ . The linear space of equivalence classes of random variables on it is denoted by  $L^0(\Omega, \mathcal{F}, P)$ , or  $L^0$  for short. We always equip such a space with the  $P$ -almost sure order. For  $p \in (0, \infty)$ , the linear space of equivalence classes of  $p$ -integrable random variables is denoted by  $L^p(\Omega, \mathcal{F}, P)$ , or  $L^p$  for short. Further, we denote the linear space of all essentially bounded random variables by  $L^\infty(\Omega, \mathcal{F}, P)$ , or  $L^\infty$  for short. From now on, we assume a linear subspace  $\mathcal{X}$  of  $L^0$ .

Now, we state the definition of (monetary) risk measures. Our definition is consistent with Cheridito and Li (2009, Definition 2.1) and Geissel et al. (2018, Definition 1.1).

**Definition C.1** (Monetary risk measures). *A function  $\rho : \mathcal{X} \rightarrow (-\infty, \infty]$  is called a monetary risk measure, if for all  $X, Y \in \mathcal{X}$  the following properties hold:*

- (i) *Finiteness at 0:  $\rho(0) \in \mathbb{R}$ .*
- (ii) *Monotonicity:  $X \leq Y$  implies  $\rho(X) \geq \rho(Y)$ .*
- (iii) *Cash invariance: For all  $m \in \mathbb{R}$  we have  $\rho(X + m) = \rho(X) - m$ .*

*A monetary risk measure is called convex, if for all  $X, Y \in \mathcal{X}$  it holds:*

- (iv) *Convexity: For  $\alpha \in (0, 1)$  we have  $\rho(\alpha X + (1 - \alpha)Y) \leq \alpha\rho(X) + (1 - \alpha)\rho(Y)$ .*

*A convex monetary risk measure is called coherent, if for all  $X \in \mathcal{X}$  it holds:*

- (v) *Positive homogeneity: For  $\alpha \geq 0$  we have  $\rho(\alpha X) = \alpha\rho(X)$ .*

**Remark C.2.** Definition C.1 states that risk measures are functionals which map a financial position in form of a random variable to a key figure which should describe the risk of this financial position. Further, these functionals satisfy desirable properties from an economical point of view. We discuss these properties shortly: Monotonicity says that the capital requirement is larger for a smaller financial position. Cash invariance says that if there is a riskless ingredient in the financial position, then the capital requirement can directly be reduced by this constant payoff. Convexity describes that diversification between two financial positions reduces the capital requirement. And positive homogeneity means that a linear scaling of a financial position can also be handled by scaling the capital requirement of the unscaled financial position.

VaR, CVaR, EVaR and RVaR are monetary risk measures. We discuss the EVaR and the RVaR more in detail. First, let us state the mathematical precise definition of the EVaR.

**Definition C.3** (Expectiles and EVaR). *Let  $\alpha \in (0, 1)$ ,  $\mathcal{X} \subset L^1$  and  $X \in \mathcal{X}$ . The  $\alpha$ -expectile  $e_\alpha(X)$  of  $X$  is the unique solution of*

$$\alpha E[\max\{X - e_\alpha(X), 0\}] = (1 - \alpha)E[-\min\{X - e_\alpha(X), 0\}].$$

*The Expectile-VaR (EVaR) at level  $\alpha$  is then defined by  $\text{EVaR}_\alpha(X) := -e_\alpha(X)$ .*

**Remark C.4.** For a choice of  $\alpha \leq \frac{1}{2}$ , the EVaR is a coherent monetary risk measure, see e.g., Bellini and Di Bernardino (2017). Moreover, expectiles are the only generalized quantiles that lead to coherent monetary risk measures, see Bellini et al. (2014, Proposition 6).

Now, we state another interpretation of expectiles. They are special cases of the *zero utility premium principle*. Therefore, we assume a loss function  $l : \mathbb{R} \rightarrow \mathbb{R}$  satisfying specific properties<sup>1</sup> and a random variable  $X \in \mathcal{X}$  representing the profit and loss of an agent at a future time point. The zero utility premium principle states that the premium  $p$  for covering  $X$  should satisfy the following equation:

$$E[l(-X - p)] = 0.$$

Expectiles are the special case in which  $l$  is given by the following relation with respect to a scalar  $\alpha \in (0, 1)$ :

$$l(x) = \begin{cases} (1 - \alpha)x & , x > 0, \\ \alpha x & , x \leq 0. \end{cases}$$

Now, we prove properties of the function  $h_{X,\alpha}$ , which we already mentioned in Section 3.1. If the lower and upper bounds of a distribution lead to different signs with respect to the function  $x \mapsto h_{X,\alpha}(x) - x$ , then they are suitable as starting points for the bisection search algorithm. The upcoming result states that this situation is satisfied.

Note, on a quantum computer we use circuits to describe bounded distributions, which act as approximations for unbounded distributions. Hence, it is enough to state the upcoming result only for bounded random variables. Further, for this result, we denote the essential infimum, respectively the essential supremum, of a random variable  $X$  by  $\text{ess inf } X$ , respectively  $\text{ess sup } X$ .

**Proposition C.5** (Starting values for bisection search algorithm). *Let  $\alpha \in \left[\frac{1}{2}, 1\right)$  and  $X \in L^\infty$ . Then it holds that*

$$h_{X,\alpha}(\text{ess inf } X) \geq \text{ess inf } X \quad \text{and} \quad h_{X,\alpha}(\text{ess sup } X) \leq \text{ess sup } X.$$

---

<sup>1</sup>For instance, Föllmer and Schied (2016, Definition 4.111) define a loss function to be increasing and not identically constant.

*Proof:* For the essential infimum we obtain

$$h_{X,\alpha}(\text{ess inf } X) - \text{ess inf } X = \frac{\alpha}{1-\alpha} (E[X] - \text{ess inf } X) \geq 0.$$

For the essential supremum it holds that

$$h_{X,\alpha}(\text{ess sup } X) - \text{ess sup } X = E[X] - \text{ess sup } X \leq 0.$$

□

**Proposition C.6** (Continuity of  $h_{X,\alpha}$ ). *Let  $\alpha \in [\frac{1}{2}, 1)$  and  $X \in L^1$ . The function  $h_{X,\alpha}$  is continuous with respect to the Euclidean norm.*

*Proof:* Assume an arbitrary sequence  $\{x_n\} \subset \mathbb{R}$  which converges to a point  $x \in \mathbb{R}$ . Then the sequence  $\{Y_n\}$  defined by

$$Y_n = \max \{(1 + \beta) X - \beta x_n, X\} \in L^1,$$

converges pointwise to

$$Y = \max \{(1 + \beta) X - \beta x, X\} \in L^1.$$

Furthermore, we have for each  $n \in \mathbb{N}$  that

$$|\max \{(1 + \beta) X - \beta x_n, X\}| \leq |X| + |\beta| \max \left\{ X - \min_{n \in \mathbb{N}} x_n, 0 \right\} \in L^1.$$

Hence, by dominated convergence  $Y_n \xrightarrow{L^1} Y$ , i.e.,  $E[Y_n] \rightarrow E[Y]$  and we obtain that  $h_{X,\alpha}$  is continuous. □

For the sake of completeness, we also state the mathematical precise definition of the RVaR, which is orientated on Fissler and Ziegel (2021, Definition 2.1).

**Definition C.7** (Range Value-at-Risk). *The Range Value-at-Risk (RVaR) of a payoff  $X \in \mathcal{X} \subset L^1$  at levels  $0 < \alpha < \beta < 1$  is defined by<sup>2</sup>.*

$$\text{RVaR}_{\alpha,\beta}(X) := \frac{1}{\beta - \alpha} \int_{\alpha}^{\beta} \text{VaR}_u(X) \, du.$$

**Remark C.8.** We obtain the following limit behavior:  $\lim_{\alpha \uparrow \beta} \text{RVaR}_{\alpha,\beta}(X) = \text{VaR}_{\beta}(X)$ , i.e., the RVaR converges to the VaR at level  $\beta$  for  $\alpha \rightarrow \beta$ . The Range Value-at-Risk is not coherent, due to the missing convexity.

---

<sup>2</sup>Here,  $\text{VaR}_{\lambda}(X)$  refers to the negative upper quantile function of a random variable  $X$  at level  $\lambda$ . For more information about quantile functions we refer to Föllmer and Schied (2016, Appendix A.3).